Article

A DC Arc Fault Detection Method Based on AR Model for Photovoltaic Systems

Yao Wang [1,2,3], Xiang Li [1,2], Yunsheng Ban [4,*], Xiaochen Ma [1,2], Chenguang Hao [1,2], Jiawang Zhou [1,2] and Huimao Cai [5]

1　State Key Laboratory of Reliability and Intelligence of Electrical Equipment, Hebei University of Technology, Tianjin 300132, China
2　Key Laboratory of Electromagnetic Field and Electrical Apparatus Reliability of Hebei Province, Hebei University of Technology, Tianjin 300132, China
3　Yangtze Delta Region Center of Electrical Engineer Innovation, Wenzhou 325600, China
4　Beijing Qixing Huachuang Flowmeter Co., Ltd., Beijing 102600, China
5　Zhejiang PEOPLE Electric Appliance Co., Ltd., Wenzhou 325600, China
*　Correspondence: banyslh@163.com

Abstract: DC arc faults are dangerous to photovoltaic (PV) systems and can cause serious electric fire hazards and property damage. Because the PV inverter works in a high-frequency pulse width modulation (PWM) control mode, the arc fault detection is prone to nuisance tripping due to PV inverter noises. An arc fault detection method based on the autoregressive (AR) model is proposed. A test platform collects the database of this research according to the UL1699B standard, in which three different types of PV inverters are taken into consideration to make it more generalized. The arc current can be considered a nonstationary random signal while the noise of the PV inverter is not. According to the difference in randomness features between an arc and the noise, a detection method based on the AR model is proposed. The Burg algorithm is used to determine model coefficients, while the Akaike Information Criterion (AIC) is applied to explore the best order of the proposed model. The correlation coefficient difference of the model coefficients plays a role as a criterion to identify if there is an arc fault. Moreover, a prototype circuit based on the TMS320F28033 MCU is built for algorithm verification. Test results show that the proposed algorithm can identify an arc fault without a false positive under different PV inverter conditions. The fault clearing time is between 60 ms to 80 ms, which can meet the requirement of 200 ms specified by the standard.

Keywords: DC series arc fault; arc fault detection; autoregressive model; photovoltaic systems

1. Introduction

Due to the huge demand for clean energy, the application of photovoltaic (PV) systems has been increasing rapidly [1–4]. It is expected that solar photovoltaic installations will reach 800 GW by 2021 [5]. Unfortunately, PV systems are prone to suffer electrical fire hazards because of arc faults on the DC side. There is no natural zero-crossing in the DC current, which results in the relevant fault arcing being difficult to extinguish by itself [6,7]. According to the relationship between arcs and PV inverters, arc faults can be categorized as series and parallel ones. Compared with the parallel fault arc, due to the series connection with the photovoltaic inverter, the current of the PV inverters will decrease rather than increase, which is more challenging for the fault diagnosis [8]. The noise of the PV inverters is generally below 10 kHz. At the same time, the high-frequency characteristic signals caused by the arc are typically concentrated in the 10–80 kHz frequency band, the high-frequency characteristic of a series arc covers the noise of the photovoltaic inverter [9]. However, conventional protection devices used for overcurrent or leakage current protection cannot function well in the event of a series arc fault [10].

Different methods have been proposed to solve this issue. The arc current signals are most commonly used for fault detection due to their independence of where the arc occurs. The arcs usually show transient and random changes in the current, which can be described by indexes in time, frequency, or time-frequency domains [11]. Sultana [12] proposed an arc fault detection method for DC series arcs, which uses three windows (scanning windows) running over the electrical current waveform. Chen. S [13] uses the unstable fluctuation in the time domain and extra arc noise in the time-frequency domain as identification features for arc fault detection. Liu. S [14] proposed a time and time-frequency domain analysis method combining the loop current and the PV-side voltage for detecting the series DC arc fault. Fenz. W [15] presented a novel approach to detect arcs in DC microgrids via their high-frequency spectral pattern using ideas from compressed sensing. Park. H. P [16] proposed an arc fault detection algorithm based on the relative comparison of current variability according to the frequency spectrum and time series. Xiong [17] investigated the difference in the integrated Fast Fourier Transform (FFT) of the current signal by a Rogowski coil correlates with the series faults. Navalpakkam [18] presented a novel approach based on voltage differential protection to detect the series arc faults. A commercial arc fault detection evaluation board for PV systems has been released by Texas Instruments Inc., which is using the Fast Fourier Transform algorithm [19]. This method can easily be implemented by hardware and can be applied by most commercial arc fault detection products. However, interference noise in PV systems sometimes exhibits similar features to the arc signal in the time or frequency domain, resulting in nuisance tripping.

Artificial Intelligence (AI) based methods provide new ideas for DC arc fault detection. Unlike traditional methods, the AI-based method is robust to the influence of Maximum Power Point Tracking (MPPT) controls or switch operations on the current. Liu. S [20] proposed domain adaptation combined with a deep convolutional generative adversarial network (DA-DCGAN)-based methodology for DC series arc fault diagnosis. Yang [21] employed Back Propagation Neural Network for the detection of DC fault arcs. E. Pedersen [22] adopted the radial basis networks to identify the DC arc faults. Vu Le [23] proposed a method based on ensemble machine learning algorithms to detect series DC arc faults. Momoh [24] uses the Fourier transformation to analyze the DC arcing fault signals, and design an artificial neural network to detect an arcing fault. Omran [25] proposed an intelligent classification method based on a convolution neural network for the detection of DC arc faults. Cao established the relevance vector machine (RVM) model to identify specific fault types [26].

Although AI-based methods have improved detecting accuracy, they typically require big data, complicated data cleaning, and model training processes. The main contribution of this paper is to investigate the essential differences in stochastic characteristics between the DC arc faults and PV inverter noise. The stochastic characteristics of the arc current can be demonstrated by a series of coefficients of its power spectral density (PSD), just as with the FFT-based method. We use the autoregressive (AR) model to obtain these coefficients. Since the stochastic characteristics are inherent attributes of an arc while the PV inverter noise is usually stable in a short time interval, it is convenient to set a unique threshold for arc fault detection.

The rest of this article is organized as follows. Section 2 builds a test platform according to the UL1699B-2018 standard, then analyzes the influence of working current noises. Section 3 sets up the AR model which has the best order for the arc-fault random signals after a comparative analysis. Section 4 proposes the arc detection method by the AR model and AIC criterion. The experimental results are discussed in Section 5. Finally, the conclusion is given in Section 6.

2. Analysis of DC Arc Fault Characteristics of PV System

2.1. DC Arc Fault Test Platform for PV System

Since the DC arc faults in PV systems occur randomly on site, which are difficult to be captured or reproduced, a specific test platform is required to generate arc faults

under different operating conditions. As per the UL1699B standard, a DC arc fault test platform is built, including PV arrays/simulators, arc generators, and PV inverters, as shown in Figure 1. A PV array with two strings in parallel is used for the tests, which will make the data collection more convincing. The maximum output power for each string is 10 kW. Meanwhile, a Chroma brand PV simulator with a rated power of 15 kW is also applied to make the tests more convenient and diversified, capable of simulating different I–V curves under various weather conditions such as irradiation, temperature, rain, and shaded by trees or clouds. At the same time, the potential influence of parasitic capacitance and parasitic inductance of DC transmission line on arc current detection should be considered, and impedance networks are added in the middle of photovoltaic strings. The resistance and capacitance parameters of the impedance network are shown in Table 1. An arc generator is integrated with the system to produce series arc faults, which are usually caused by loose connections of metal terminals.
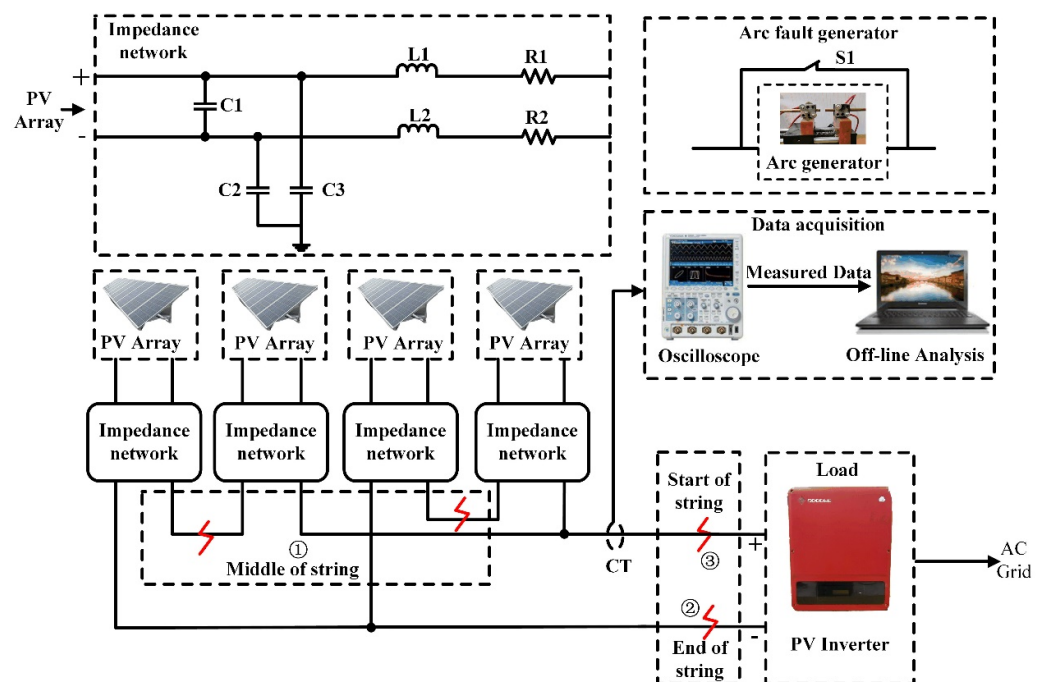

Figure 1. DC arc test platform.

Table 1. Impedance network parameter setting.

Component	Parameter Value
C1	20 μF
C2, C3	22 nF
L1, L2	25 μH
R1, R2	1 Ω

According to the requirement of UL1699B, the arc fault detection device (AFDD) for PV systems can be categorized into two types, including the embedded type and the external type. The embedded type AFDD can be integrated with a PV inverter, combiner box, or DC-DC converter, which means that AFDD is usually used for a specific PV inverter. On the contrary, the external type AFDD is more generalized in the application, and it has to be adapted to different brands of PV inverters. Therefore, we are working on the external type AFDD, and three different inverters are applied for this research, as shown in Table 2.

Table 2. Detailed parameters for the test platform.

Load	Voltage/Current	Gap	Speed
PV Inverter #A	490 V/7 A	0.8 mm	
	810 V/14 A	1.1 mm	
PV Inverter #B	490 V/7 A	0.8 mm	
	810 V/14 A	1.1 mm	5 mm/s
PV Inverter #C	490 V/7 A	0.8 mm	
	810 V/14 A	1.1 mm	

In addition, the arc generator comprises a pair of stationary and moving electrodes, which can be driven by a stepper motor to move separately at a constant speed of 5 mm/s to initiate arcs. The electrodes are made of copper bars with a diameter of 6.35 mm (1/4 inch) according to UL 1699B. Figure 2 shows a close-up view of the arc generator. While Table 2 shows the maximum air gaps of the electrodes under different arc currents.
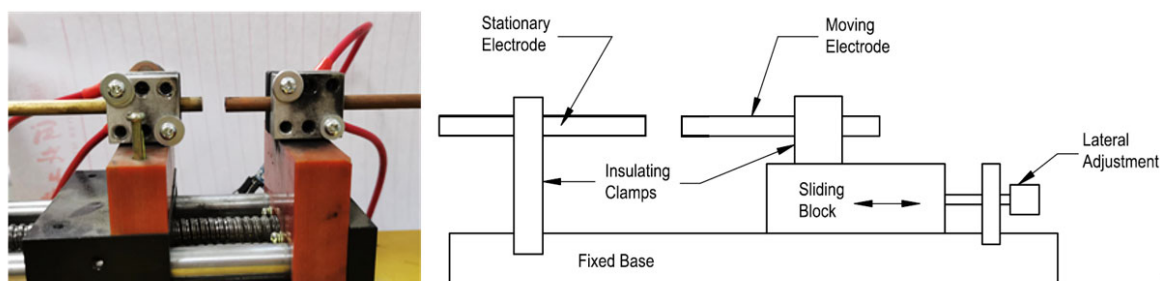

Figure 2. The close-up view of the arc generator.

2.2. The Influence of Working Current Noise of PV System on Fault Detection

Whether from the perspective of time or frequency domains, the DC arc current in PV systems will show high-frequency strikes, especially within the bandwidth of 100 kHz. However, PV inverters will introduce similar noises to the current due to their PWM operation, the amplitude of which may be the same as or even higher than that of arc signals. As a result, it will be difficult to distinguish the arc fault from the normal operation using the amplitude differences.

DC arc is an inherently random phenomenon that can be observed even in a short time window of a few milliseconds, while PWM noise is rhythmic due to periodic modulation and system inertia. Therefore, the random behavior of DC arcs can be used for arc fault detection.

Due to its PWM control, the PV inverter emits high-frequency noise to the current during normal operation. The PV inverter noise may overlap with the arc signal in frequency bandwidth, resulting in nuisance tripping. Therefore, we have to take measures to discriminate DC arcs from the normal operation of a PV system. The PSD can describe the random signals, which defines the strength of the signal's power contents as a function of frequency. Figure 3 shows the waveform and the corresponding PSD of a current time series. The PV inverter noise can be regarded as a stationary random signal within a short time slot (e.g., 10 ms) due to the inertia of the system. However, DC arcs exhibit different randomness characteristics that make them easy to distinguish from interfering signals.
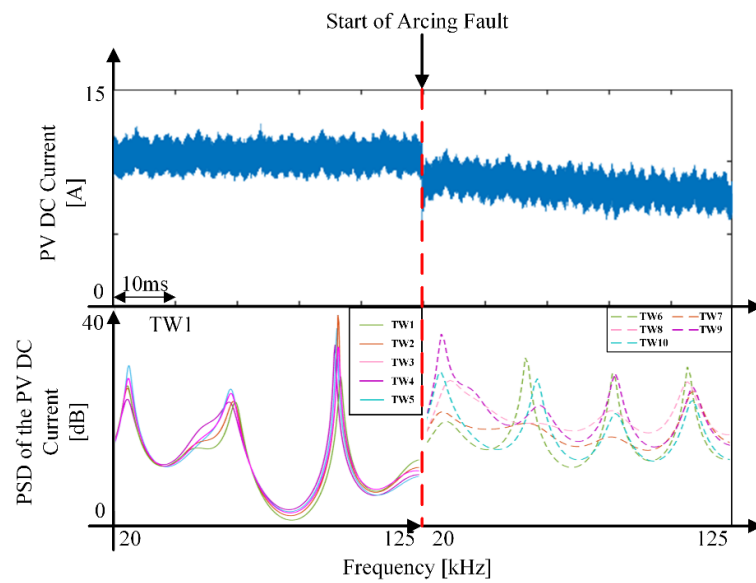
Figure 3. The PSD of measured current under normal operation and arc fault conditions (TW means time window).

3. Modeling Method of PV DC Arc Based on AR Model

3.1. Modeling Method Based on AR Model

As mentioned in Section 2.2, we can use an appropriate times series model to estimate the PSD of the inverter noise because it follows a similar pattern. However, the arc current does not apply to the model, which can be criterion for arc fault detection. There are three commonly used time series models for a stationary stochastic process, including the Autoregressive model (AR), the Moving Average (MA) model, and the integrated Autoregressive Moving Average (ARMA) model. The AR model has the simplest structure, which requires the least computation and is most suitable for the DC current processing in the PV system by using an embedded microcontroller, as shown in Table 3.

Table 3. Comparison of commonly used models for the stochastic process.

Model	Spectral Distribution	Computation	Complexity
AR	Peak	Small	Easy
MA	Trough	Moderate	Moderate
ARMA	Peak, Trough	Large	Complex

Then, the successive samples of inverter noise $x(t)$ can be modeled by an AR-based model of order p. which can be expressed by a difference equation as:

$$x(t) = -\sum_{i=1}^{p} a_p(i)x(t-i) + \varepsilon(t) \tag{1}$$

$a_p(i)\ i = (1, 2, \ldots, p)$ are the coefficients regarding the corresponding time series data. $\varepsilon(t)$ is called the error terms, which is typically a white noise with zero-mean and a variance of σ_t. In addition, $\varepsilon(t)$ is uncorrelated with the sequence $x(i)\ (i < t)$. In Equation (1), the response variable $x(t)$ is fitted by a linear combination of its previous values, which means the p-ordered AR process would be related to data p periods apart. Since the AR process can be expressed as the output of an all-pole filter, an estimated PSD of the same order p can be written as:

$$\hat{P}_X(i) = \frac{\hat{\sigma}_t^2}{\left|1 + \sum_{i=1}^{p} \hat{a}_p(i)e^{-j\omega i}\right|} \tag{2}$$

It can be seen from Equation (2) that the prediction accuracy of the PSD depends on how accurately the $\hat{a}_p(i)$ and $\hat{\sigma}_t^2$ can be estimated.

3.2. The Parameter Estimation for the AR-Based Model

Several methods can be used to fit the parameters to the measured data, such as the Burg and the Yule-Walker method. Compared with the Yule-Walker method, the Burg method is preferable and has a higher estimation resolution. The Burg method first estimates the reflection coefficients k_m by minimizing the forward and backward prediction errors, which is:

$$k_m = -2 \frac{\sum_{n=m}^{N-1} e_{m-1}^f(n) e_{m-1}^b(n-1)}{\sum_{n=m}^{N-1} \left\{ \left[e_{m-1}^f(n) \right]^2 + \left[e_{m-1}^b(n-1) \right]^2 \right\}} \tag{3}$$

In Equation (3), the e^f and e^b refer to the forward and backward prediction errors, respectively, which can be written as:

$$e_m^f(n) = e_{m-1}^f(n) + k_m e_{m-1}^b(n-1) e_m^b(n) = k_m e_{m-1}^f(n) + e_{m-1}^b(n-1) e_0^f(n) = e_0^b(n) = x(n) \tag{4}$$

Since the reflection coefficients k_m constitute unbiased estimates of the partial correlation coefficients, the autocovariance function R_x for delays 0 to p related to the parameters a_p can be derived by the Yule-Walker equation:

$$R_x(m) = \begin{cases} -\sum_{k=1}^{p} a_p(k) R_x(m-k), m \geq 1 \\ -\sum_{k=1}^{p} a_p(k) R_x(k) + \sigma_t^2, m = 0 \end{cases} \tag{5}$$

where k is $1, 2, \ldots, m-1$. According to Equations (4) and (5), the parameters a_p can be determined using the Levinson-Durbin algorithm, which can be written as:

$$a_m(k) = a_{m-1}(k) + k_m a_{m-1}(m-k) a_m(m) = k_m \tag{6}$$

Repeat the process as shown in Equation (6) until the order m equals p, so that the parameters of all orders can be obtained.

3.3. The Best Order for the AR-Based Model

Another important thing is to determine the best order for the proposed AR-based model, which entails a tradeoff of bias and variance, and a poor choice can result in a virtually useless estimator. The Akaike Information Criterion (AIC) can achieve this goal by providing an asymptotically unbiased estimate of the difference between the various fitted AR models and the truth. Furthermore, this can be carried out without knowing the true model. The AIC is defined as:

$$\text{AIC} = -\frac{2}{N} \ln L + \frac{2p}{N} \tag{7}$$

where L is the maximized likelihood and N is the sample size. p is the number of independently adjusted parameters in the candidate model. Since the proposed AR(p) model is a Gaussian one, AIC reduces to

$$\text{AIC} = \ln \hat{\sigma}_t^2 + \frac{2p}{N} \tag{8}$$

where $\hat{\sigma}_p^2$ is the maximum-likelihood estimate of $\hat{\sigma}_t^2$, which can be determined by

$$\hat{\sigma}_p^2 = \left(1 - |k_{p-1}|^2 \right) \hat{\sigma}_{p-1}^2 \tag{9}$$

where k_p is the reflection coefficient as per Equation (3). The value of the AIC represents the goodness of fit. The smaller the value is, the better the model fits the data. In order to ensure that the established model has sufficient estimation accuracy and low computational burden, it is necessary to use the measured data from PV inverters #A, #B, and #C to determine an optimal order. The original data are collected under the normal operation of inverters with a total of 4800 samples, and each sample lasts for 10 ms. According to the analysis of the generation mechanism of arc and the time-frequency domain characteristics of arc current, random characteristic is one of the typical inherent characteristics of the arc. The observation in a short time window shows that the operating noise of the inverter is relatively stable. The results of AR model estimation are consistent in normal operation. The arc signal is non-stationary and the model estimates for each window vary greatly. We used normal data to establish the AR model. Then, the AIC values can be obtained as per Equations (8) and (9) for a given order from 1 to 20, as shown in Figure 4. It can be seen from Figure 4 that the best order for the proposed AR-based model can be located at 12th, for which order we can always obtain the minimum AIC value, that is, the *p*-value is 12.
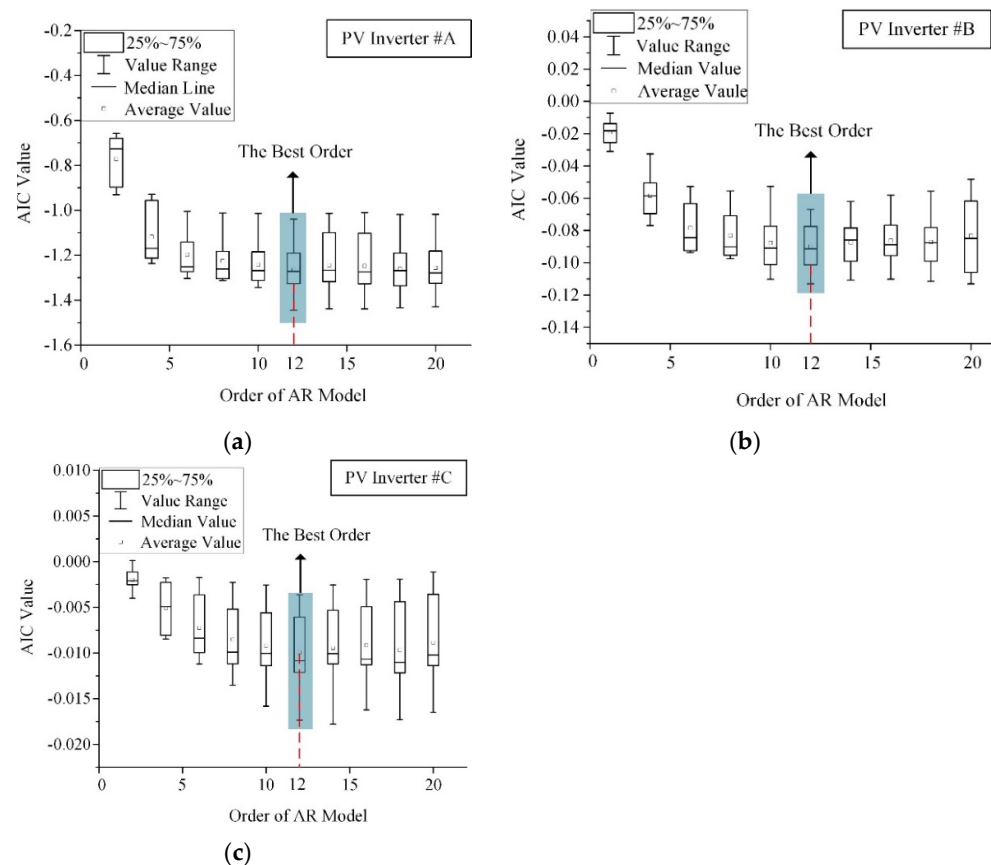

Figure 4. The AIC values of the proposed model for a given order from 1 to 20. (**a**) PV inverter #*A*; (**b**) PV inverter #*B*; (**c**) PV inverter #*C*.

4. DC Arc Fault Detection Based on the Proposed Model

4.1. Arc Fault Identification Method

Just like the FFT-based method, we can use the PSD coefficients $a_t(i)$ $(i = 1, 2, \ldots 12)$ deriving from Equation (6) to represent the corresponding time series of the measured current. According to Section 2.2, even if the arc current is observed in a short time interval, it can be regarded as a non-stationary random signal. In that case, an arc fault can be confirmed if there is a significant difference of the coefficients $a_{12}(i)$ between the two adjacent "observing time windows".

Mathematically, such a difference can be evaluated by the correlation coefficient r_i, which is defined as:

$$r_i = \frac{Cov(a_t, a_{t-1})}{\sqrt{Var[a_t] Var[a_{t-1}]}} \tag{10}$$

where a_t and a_{t-1} are the PSD coefficients at observing time windows of t and $t - 1$, respectively. Equation (10) describes how similar the PSD between the two adjacent observing time windows is. In order to avoid the interference of the inverter noise, the difference of adjacent correlation coefficients r_i and r_{i-1} can be used for the arc fault identification. If $|r_i - r_{i-1}|$ exceeds a predetermined threshold r_{th}, the PV system is probably suffering from an arc fault. This protection logic can be illustrated using the flowchart as shown in Figure 5. The detailed procedures are:

1. The DC bus current is being sampled in real-time until the data buffer is full for one observing time window. Then it goes to the next step;
2. The correlation coefficient r_i as well as the difference of $|r_i - r_{i-1}|$ are calculated in this step;
3. If $|r_i - r_{i-1}| > r_{th}$, a variable F, indicating the possibility of arc fault, will increase by a predetermined number of a. If not, the variable F will be reduced by a specific number of b. It should be noted that the number of b should be less than the number of a, so that the algorithm can deal with discontinuous arc faults. Empirically, the number of a can be 2, while the number of b can be 1;
4. If the value of the accumulator F is large enough (greater than a predetermined value δ, e.g., 12), an arc fault will be confirmed eventually.
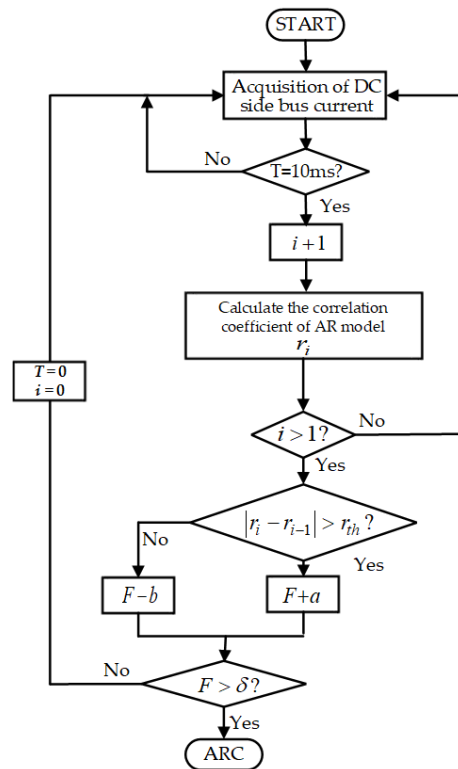

Figure 5. The flowchart of arc fault identification based on the proposed method.

4.2. Thresholds Determination for the Proposed Method

For the AR-model-based arc fault detection method, some parameters need to be determined before application. The first one is how long the observing time window should be. For a given observing time window of 1 ms to 20 ms, variances of r_i can be calculated under normal and arc fault conditions of PV inverter #A, #B and #C, respectively,

as shown in Table 4. Under normal operation conditions, the variances of all observing time windows are small, which means few changes in the PSD of inverter noises and are in accordance with the theoretical analysis of Section 2.2. On the contrary, due to the non-stationary characteristics of the arc current, the corresponding variance will become larger, which is beneficial to arc fault detection. Therefore, the preferable observing time window should make the variance of arc faults significantly greater than normal operation. Here we choose 10 ms as the best observing time window. The other parameter to be determined is the threshold r_{th}. Here plot the $|r_i - r_{i-1}|$ under all conditions in Figure 6. The values of $|r_i - r_{i-1}|$ under arc faults are significantly higher than that under normal operation no matter what type of inverter. So 0.1 is selected as the value of threshold r_{th} (normal value less than 0.05).

Table 4. The variances of r_i for a given observing time window of 1 ms to 20 ms.

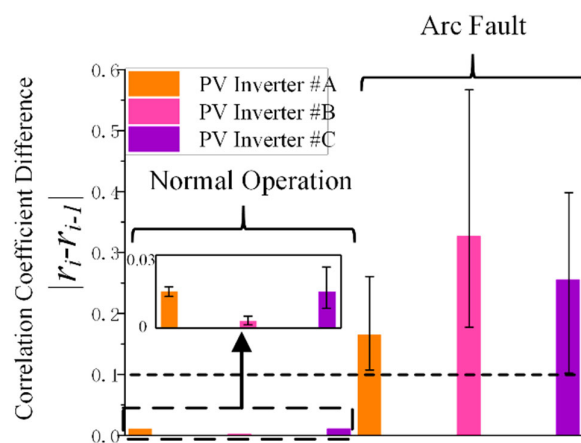| Time Window/ms	Correlation Coefficient Variance of Arc	Correlation Coefficient Variance of Normal
1	0.05939	0.01268
2	0.07528	0.00265
7	0.06233	0.00195
10	0.24262	0.00140
12	0.02257	0.00085
15	0.18921	0.00110
17	0.17401	0.00151
20	0.21711	0.00806

Figure 6. The correlation coefficient differences and threshold for the proposed method.

5. Experimental Results and Discussion

5.1. Hardware Implementation

In order to verify the feasibility of the proposed method, a Digital Signal Processor (DSP) based prototype is designed, as shown in Figure 7. A TI TMS320F28033 DSP is used for the algorithm implementation, which is a 32-bit MCU with a 60 MHz clock frequency. The hardware circuit also comprises a current transformer (CT), a bandpass filter, and an Analog-to-Digital converter (ADC). The CT is responsible for measuring the required current signal, where a Pulse PA3655NL CT is adopted. The PA3655NL is designed for arc fault detection circuits within a bandwidth of 50–500 kHz and a maximum peak current of 34 A. Moreover, a 4-order bandpass filter is designed based on a low noise precision operation amplifier of TISM73307 with a bandwidth of 33–100 kHz. An external ADC of SM73201 is combined with the MCU to guarantee a better signal quality. The SM73201 has a 16-bit resolution with a maximum sampling rate of 250 kSPS and features a differential analog input with an excellent common-mode signal rejection ratio of 85 dB, making the SM73201 suitable for noisy environments.
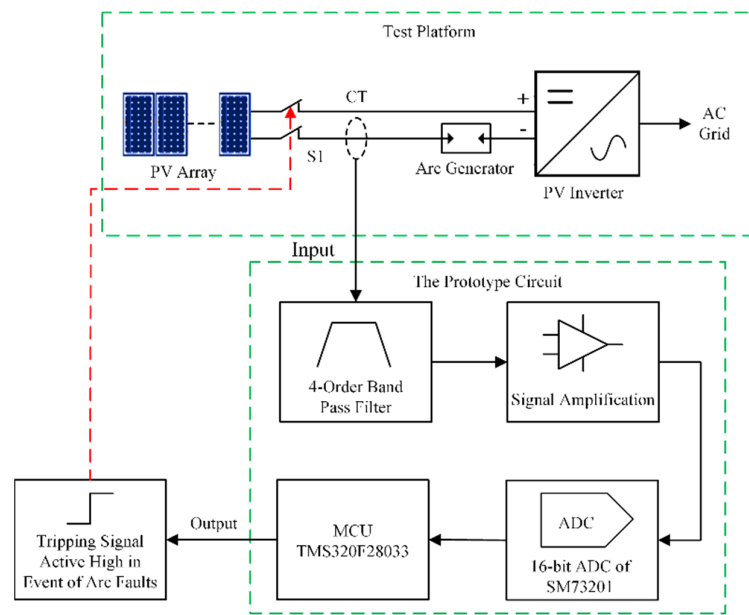
Figure 7. The functional block diagram of the proposed prototype.

5.2. Test Results and Discussion

The prototype is tested by the experimental platform mentioned in Section 2.1 as illustrated in Figure 8, and some of the corresponding results are shown in Figure 9.
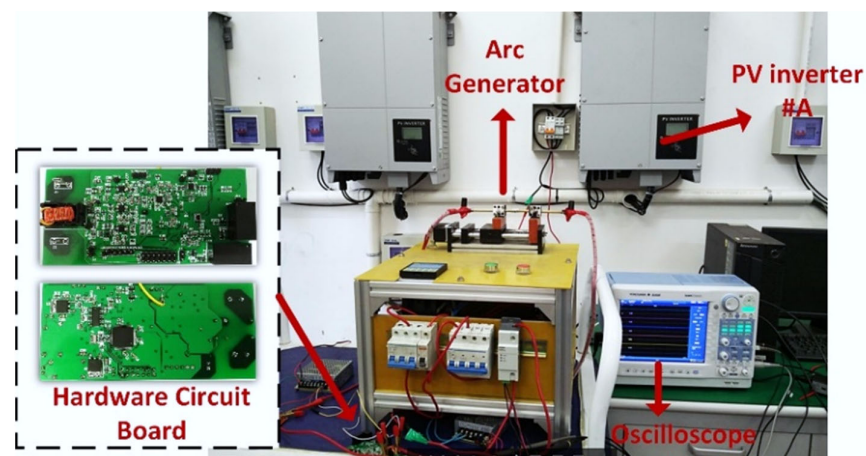

Figure 8. The prototype and the corresponding test scenario.

The absolute value of correlation coefficient difference in all cases of normal operation keeps far from the threshold r_{th} of 0.1, although there is a little ripple in some scenarios such as Figure 9a,b. The arc is random, which is manifested in that the combustion degree of the arc is not fixed (especially in the arc starting stage), and the distortion details of the signal have no fixed repetition law. The similarity of the PSD curves of the arc data of a window is used as the characteristic quantity for the judgment of the arc fault. Due to the randomness of the arc fault, the arc data in each sampling window is not completely consistent, so the correlation coefficients of the PSD curves in the adjacent windows are different.

This result shows that the inverter noises are relatively stable and comply with the theoretical analysis in Section 2.2. However, the corresponding value of $|r_i - r_{i-1}|$ will be rising dramatically in the event of an arc fault, which can reach as high as five or six times the threshold r_{th}. Therefore, an arc fault can be detected in real-time without any false positive. Test results also show that the fault clear times are between 60 ms and 80 ms, which is faster than the standard requirement of a minimum of 200 ms.
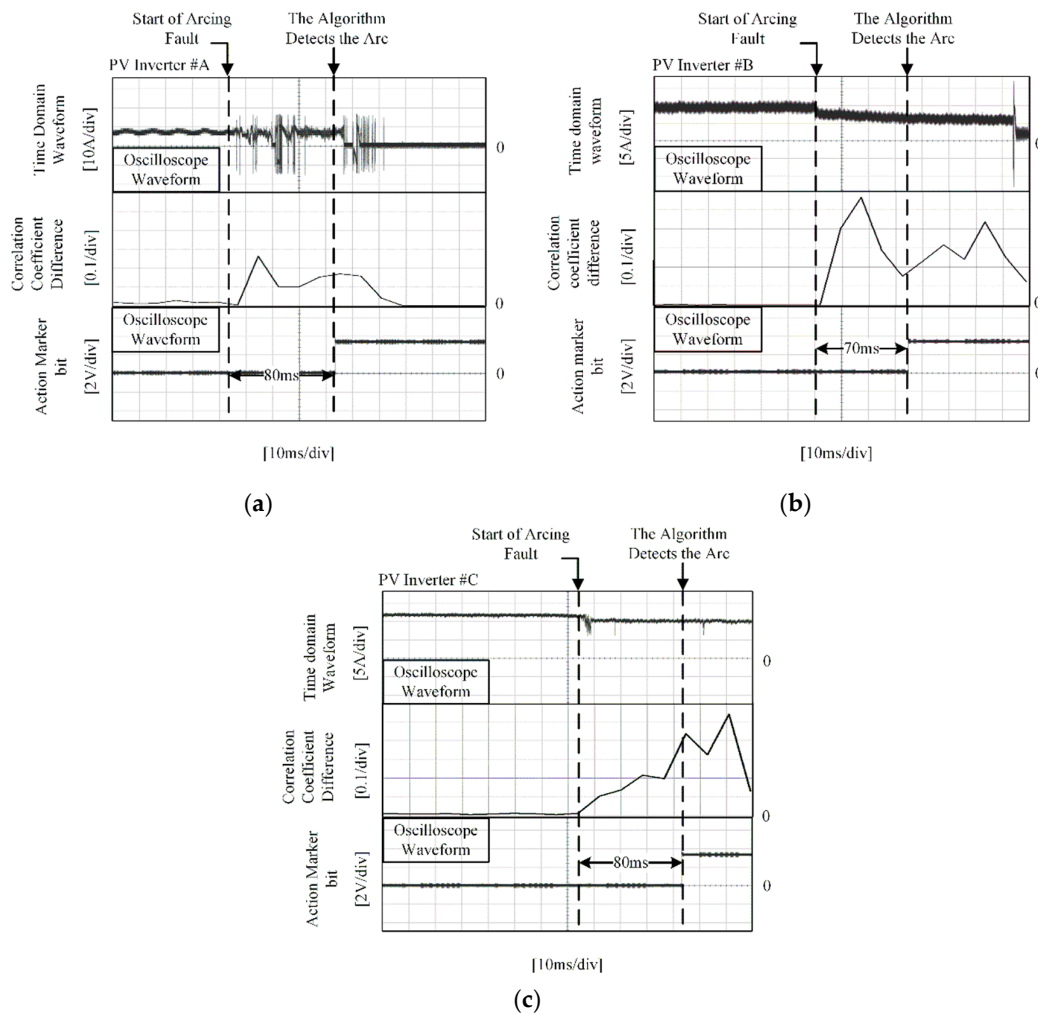
Figure 9. Test results of the designed prototype. (**a**) PV inverter #*A*; (**b**) PV inverter #*B*; (**c**) PV inverter #*C*.

As for the impact of MPPT, the corresponding data is collected as per the UL1699B standard requirement. These tests are generally conducted by varying solar irradiation or making the inverter startup. In those cases, the MPPT will be triggered and tune the operating point to a new state of maximum power output. Figure 10a is the current during the inverter starting, which includes the MPPT control process. A power spectral density (PSD) analysis using a 10 ms time window for a data partition of 50 ms in the startup process is performed, as shown in Figure 10c. It can be seen that there is almost no difference in the PSD for different time windows, reflecting that they follow a uniform randomness characteristic. Therefore, the proposed method can effectively distinguish the influence of the MPPT control from a real arc fault.

In general, the above test results verify that the proposed method can fulfill the standard requirements for PV arc fault detection under different PV inverter conditions. Furthermore, it can be embedded in an MCU-based hardware circuit for real applications as well. However, the method is only validated under standard test conditions, and more application scenarios will be considered for generalization evaluation in future work.
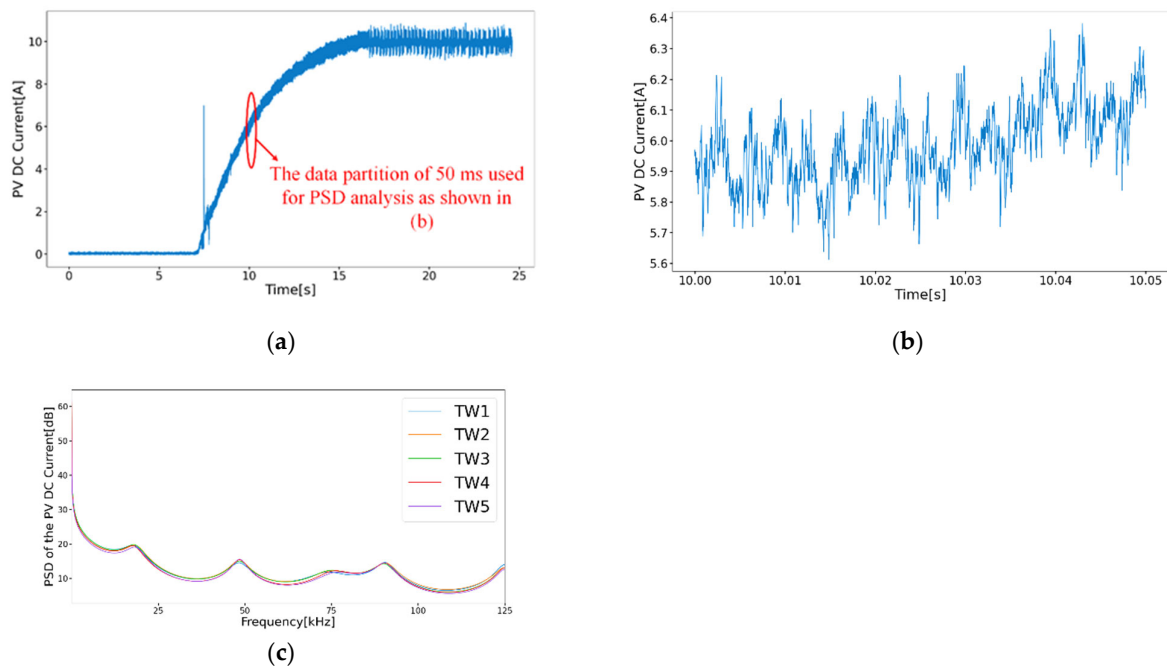
(a)

(b)

(c)

Figure 10. The current and corresponding PSD analysis of the startup process of a PV system. (**a**) The current during the inverter starting; (**b**) The data partition of 50 ms in the startup process of the PV system; (**c**) The current and corresponding PSD analysis of the startup process of a PV system.

5.3. A Comparison with Existing Methods

The main contribution of the method proposed in this paper is to apply the inherent randomness characteristics of DC arcs to arc fault detection through an AR model-based method.

Compared with the traditional methods, the proposed method has improved anti-interference capability with almost no increase in computational complexity. Therefore, it is suitable for cost-sensitive applications implemented by an industrial MCU (for instance, TMS320F28033). While compared to the AI-based method, the method in the paper needs significantly fewer computations to achieve nearly the same performance under interference conditions since it does not require big data.

Comparative tests have been conducted on the TI RD195 evaluation board, an open-source solution available [19]. It can be seen from the test result (Figure 11) that the current changes due to the varying solar irradiation caused a nuisance trip to the RD195 evaluation board. However, the proposed method is immune to this interference. Table 5. summarizes the comparative analysis of the proposed method and other methods. It can be seen that the proposed method based on the AR model has a relatively small computation amount and strong anti-interference ability.
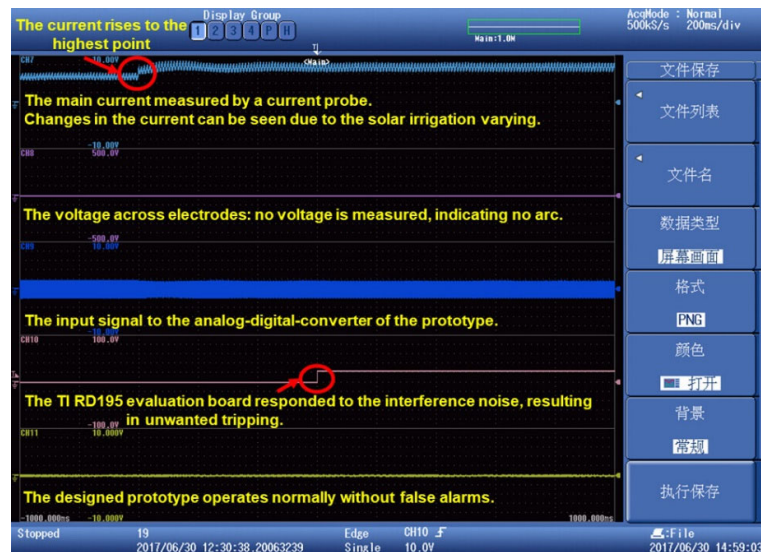
Figure 11. The test results of the traditional and the proposed method.

Table 5. Comparison of AR model method with other methods.

Particulars	Texas Instruments et al. [19]	J.A. Momoh et al. [24]	Alaa Hamza Omran et al. [25]	Ours
Method	Fast Fourier Transform Algorithm	Fast Fourier transformation and artificial neural network	Redesigning the structure of CNN in a specific form (Adding more layers to the traditional model of the CNN)	AR model based on random characteristics of DC arc
Interference Immunity	☹	☺	☺	☺
Computational Complexity	Small	Large	Large	Medium
Big Data Required	No	Yes	Yes	Yes
Suitable for Industrial MCU	Yes	No	No	Yes

6. Conclusions

In this paper, an AR model-based arc fault detection method is proposed for PV systems. Major conclusions are summarized as follows:

1. The current under arc fault and normal operating conditions of PV inverters are collected with 4800 samples, and each sample lasts for 10 ms. From the stochastic process perspective, the PV inverter noise can be regarded as a stationary random signal due the system's inertia. However, the DC arc does not follow this rule even if observed in a short time interval (e.g., 10 ms);

2. Accordingly, an AR model is built to describe such a difference. The Burg algorithm can be used to determine the model coefficients. Moreover, the model's best order can be evaluated by the AIC method, which is 12 orders. The correlation coefficient difference of the model is used as a criterion for arc fault detection, a threshold for which is chosen to be 0.1 empirically;

3. Additionally, a prototype circuit based on TMS320F28033 MCU is designed for algorithm verification. Test results show that the proposed algorithm can confirm an arc fault without a false positive under different test conditions. Besides, compared with the minimum 200 ms required by the standard, the fault clearing time is fast enough, ranging from 60 ms to 80 ms.

Author Contributions: Conceptualization, Y.W. and Y.B.; methodology, Y.W., X.L. and Y.B.; software, X.L., X.M. and J.Z.; validation, X.L., Y.B. and C.H.; formal analysis, Y.W., H.C. and X.M.; investigation,

Institutional Review Board Statement: Not applicable.

Informed Consent Statement: Not applicable.

Data Availability Statement: Not applicable.

Conflicts of Interest: The authors declare no conflict of interest.

References

1. Mishra, P.; Pradhan, A.K.; Bajpai, P. Adaptive distance relaying for distribution lines connecting inverter-interfaced solar pv plant. *IEEE Trans. Ind. Electron.* **2021**, *68*, 2300–2309. [CrossRef]
2. Alzahrani, S.; Shah, R.; Mithulananthan, N. Exploring the dynamic voltage signature of renewable rich weak power system. *IEEE Access* **2020**, *8*, 529–542. [CrossRef]
3. Artale, G.; Cataliotti, A.; Cosentino, V.; Di Cara, D.; Nuccio, S.; Tine, G. Arc fault detection method based on czt low-frequency harmonic current analysis. *IEEE Trans. Instrum. Meas.* **2017**, *66*, 888–896. [CrossRef]
4. Leva, S.; Nespoli, A.; Pretto, S.; Mussetta, M.; Ogliari, E.G.C. PV plant power nowcasting: A real case comparative study with an open access dataset. *IEEE Access* **2020**, *8*, 428–440. [CrossRef]
5. M. BOSTON. Available online: https://www.luxresearchinc.com/press-releases/solar-photovoltaic-installations-will-double-to-800-gwby-2021-as-annual-installations-reach-107-gw (accessed on 5 July 2022).
6. Xiong, Q.; Ji, S.; Zhu, L.; Zhong, L.; Liu, Y. A novel dc arc fault detection method based on electromagnetic radiation signal. *IEEE Trans. Plasma Sci.* **2017**, *45*, 472–478. [CrossRef]
7. Li, K.; Zhao, S.; Wang, Y. A planar location method for dc arc faults using dual radiation detection points and dann. *IEEE Trans. Instrum. Meas.* **2020**, *69*, 5478–5487. [CrossRef]
8. Flicker, J.; Johnson, J. Electrical simulations of series and parallel pv arc-faults. In Proceedings of the 2013 IEEE 39th Photovoltaic Specialists Conference (PVSC), Tampa, FL, USA, 16–21 June 2013; pp. 3165–3172.
9. Chen, S.; Li, X.; Xie, Z.; Meng, Y. Time–frequency distribution characteristic and model simulation of photovoltaic series arc fault with power electronic equipment. *IEEE J. Photovolt.* **2019**, *9*, 1128–1137. [CrossRef]
10. Klement, K. DC arc flash studies for solar photovoltaic systems: Challenges and recommendations. *IEEE Trans. Ind. Appl.* **2015**, *51*, 4239–4244. [CrossRef]
11. Pillai, D.S.; Blaabjerg, F.; Rajasekar, N. A comparative evaluation of advanced fault detection approaches for pv systems. *IEEE J. Photovolt.* **2019**, *9*, 513–527. [CrossRef]
12. Sultana, Q.; Mishra, P.; Chary, S. Novel control methodology for detecting series arc in dc circuits. In Proceedings of the 2017 IEEE Second International Conference on DC Microgrids (ICDCM), Nürnberg, Germany, 27–29 June 2017; pp. 12–17.
13. Chen, S.; Li, X.; Xiong, J. Series arc fault identification for photovoltaic system based on time-domain and time-frequency-domain analysis. *IEEE J. Photovolt.* **2017**, *7*, 1105–1114. [CrossRef]
14. Liu, S.; Dong, L.; Liao, X.; Cao, X.; Wang, X.; Wang, B. Application of the variational mode decomposition-based time and time–frequency domain analysis on series dc arc fault detection of photovoltaic arrays. *IEEE Access* **2019**, *7*, 177–190. [CrossRef]
15. Fenz, W.; Thumfart, S.; Yatchak, R.; Roitner, H.; Hofer, B. Detection of arc faults in pv systems using compressed sensing. *IEEE J. Photovolt.* **2020**, *10*, 676–684. [CrossRef]
16. Park, H.P.; Chae, S. DC series arc fault detection algorithm for distributed energy resources using arc fault impedance modeling. *IEEE Access* **2020**, *8*, 39–46. [CrossRef]
17. Xiong, Q.; Feng, X.; Gattozzi, A.L.; Liu, X.; Zheng, L.; Zhu, L.; Ji, S.; Hebner, R.E. Series arc fault detection and localization in dc distribution system. *IEEE Trans. Instrum. Meas.* **2020**, *69*, 122–134. [CrossRef]
18. Ananthan, S.N.; Bastos, A.F.; Santoso, S.; Feng, X.; Penney, C.; Gattozzi, A.; Hebner, R. Signatures of series arc faults to aid arc detection in low-voltage dc systems. In Proceedings of the 2020 IEEE Power Energy Society General Meeting (PESGM), Montreal, QC, Canada, 2–6 August 2020; pp. 1–5.
19. Texas Instruments. Available online: https://www.ti.com/lit/pdf/spry209 (accessed on 5 July 2022).
20. Lu, S.; Sirojan, T.; Phung, B.T.; Zhang, D.; Ambikairajah, E. DA-DCGAN: An effective methodology for dc series arc fault diagnosis in photovoltaic systems. *IEEE Access* **2019**, *7*, 831–840. [CrossRef]

21. Yang, J.; Wang, Y. Identification and detection of dc arc fault in photovoltaic power generation system. In Proceedings of the 2020 International Conference on Intelligent Transportation, Big Data Smart City (ICITBS), Vientiane, Laos, 11–12 January 2020; pp. 440–444.

22. Pedersen, E.; Rao, S.; Katoch, S.; Jaskie, K.; Spanias, A.; Tepedelenlioglu, C.; Kyriakides, E. PV array fault detection using radial basis networks. In Proceedings of the 2019 10th International Conference on Information, Intelligence, Systems and Applications (IISA), Patras, Greece, 15–17 July 2019; pp. 1–4.

23. Le, V.; Yao, X.; Miller, C.; Tsao, B.H. Series dc arc fault detection based on ensemble machine learning. *IEEE Trans. Power Electron.* **2020**, *35*, 7826–7839. [CrossRef]

24. Momoh, J.; Button, R. Design and analysis of aerospace dc arcing faults using fast fourier transformation and artificial neural network. In Proceedings of the 2003 IEEE Power Engineering Society General Meeting (IEEE Cat. No.03CH37491), Toronto, ON, Canada, 13–17 July 2003; Volume 2, pp. 788–793.

25. Omran, A.H.; Mat Said, D.; Hussin, S.M.; Mirsaeidi, S.; Abid, Y.M. An intelligent classification method of series arc fault models using deep learning algorithm. In Proceedings of the 2020 IEEE International Conference on Power and Energy (PECon), Penang, Malaysia, 7–8 December 2020; pp. 44–48.

26. Cao, C.; Xu, J.Y.; Lin, X.; Li, X.L. State Diagnosis Method of Transformer Winding Deformation Based on Fusing Vibration and Reactance Parameters. *IET Electr. Power Appl.* **2020**, 818–826.